Key Engineering Materials
ISSN: 1662-9795, Vol. 926, pp 389-400
doi:10.4028/p-lm7s8y

Submitted: 2021-11-30
Revised: 2022-01-17
Accepted: 2022-01-28
Online: 2022-07-22

Process Stability and Reproducibility of the Dieless Drawing Process for AZ31 Magnesium Wires

Merle Braatz[1,a,*], Jan Bohlen[1,b] and Noomane Ben Khalifa[1,2,c]

[1]Institute of Material and Process Design, Helmholtz-Zentrum Hereon, Max-Planck-Str. 1, 21502 Geesthacht, Germany

[2]Institute of Product and Process Innovation, Leuphana Universität Lüneburg, Universitätsallee 1, 21335 Lüneburg, Germany

[a]merle.braatz@hereon.de, [b]jan.bohlen@hereon.de, [c]noomane.ben_khalifa@leuphana.de

Keywords: magnesium wire, hot forming, dieless wire drawing, cold wire drawing, process stability

Abstract. Magnesium (Mg)-based wires are in the focus of interest for numerous applications like micro-forming technologies or medical engineering. Manufacturing thin Mg-based wires is widely realized by applying a conventional multiple pass cold wire drawing process. This requires a complex manufacturing schedule of multiple passes with intermediate heat treatments to overcome work hardening, because of the cold forming process. Especially Mg and its alloys are known for their rather low formability at room temperature associated with the hexagonal close-packed lattice structure. The dieless drawing process uses local heating to initialize a localized plastic zone under an external tensile load to achieve higher reductions in diameter in a single wire drawing pass. It can therefore present a solution for a more efficient warm manufacturing process of Mg-based wires.

In this study, the stability of the steady state material flow during a dieless wire drawing process and its reproducibility was investigated. For this purpose, a variation of process parameters was selected and wire manufacturing was carried out using magnesium alloy AZ31. A single and double dieless drawing process was applied. Additionally, a conventional cold wire drawing process including a die with the same forming schedule was executed as a benchmark experiment.

The results of this study show, that the dieless drawing process is not only a stable process after reaching the steady state, but it is also a reproducible and accurately adjustable process. Moreover, the dieless drawing process maintains the property profile of the starting material to a large extend.

Introduction

The dieless wire drawing (DD) process was first introduced in 1969 [1] and experimentally analyzed in 1975 [2]. It is described as a non-contact process for manufacturing bars, tubes and wires by using local heating to initialize a localized plastic deformation zone. Early studies with steel wires describe the potential to continuously produce wires, but also the sensitivity of the DD process to its parameter settings and therefore its overall stability [3, 4, 5]. Later studies confirm the feasibility of the DD process for Magnesium (Mg)-based wires and describe the existence of a nonstable and a steady state phase [6, 7, 8]. Milenin et al. [9] propose a multiple pass DD process to improve the stability of deformation and increase the workability. Nevertheless, only few investigations of the steady state exist and an assessment of reproducibility and process stability have not yet been investigated.

Besides lightweight applications, Mg-based products such as wires are in the focus for application in medical engineering as resorbable implant materials with good biocompatibility, whereby the mechanical properties and the surface quality of the wires are subject to special production requirements [10]. A conventional cold wire drawing (CCD) process can produce Mg-based wires that have appropriate surface quality due to the drawing die, but the material can be contaminated by abrasion or the use of lubricants, and large reductions in diameter per drawing pass are not possible [11]. Due to the hexagonal lattice structure and the associated rather low ductility, Mg-based wires are produced in multiple pass approaches with intermediate heat treatment or preferably at higher process temperatures – e.g. with the DD process.

Dieless Wire Drawing

In Fig. 1, the principle of the DD process is shown. The wire moves into the process with the feeding velocity V_0 and is drawn with the drawing velocity V_1. In the heating zone 1, an induction coil heats the wire locally. Subsequently, the wire is passively cooled to room temperature by the surrounding air of cooling zone 2. The ratio between the process velocities V_0/V_1 in combination with the local heating initializes a localized plastic deformation zone. Under the globally applied tensile load F, resulting from the difference in velocities V_0/V_1, the reduction of the cross sectional area (csa) from an initial A_0 to A_1 after the drawing pass is initiated.

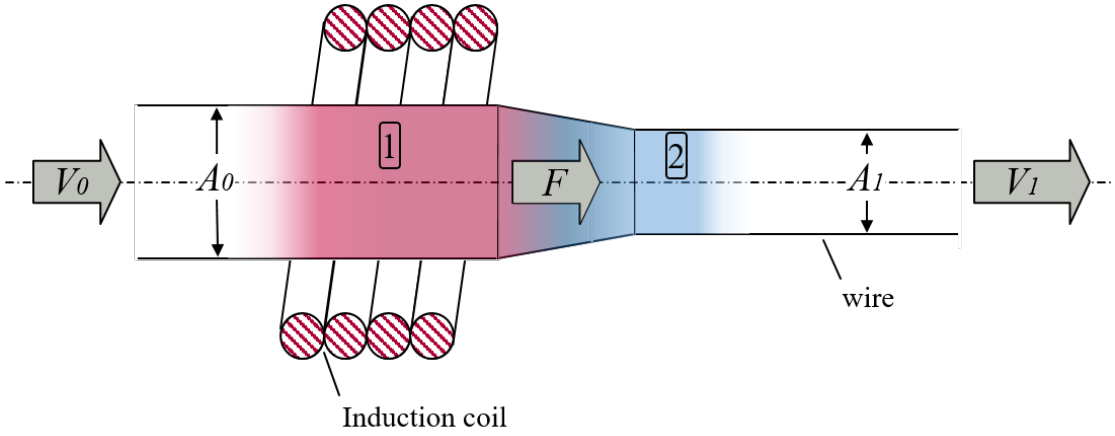

Figure 1. Schematic illustration of the dieless drawing process

Following the assumption of a constant volume, the law of continuity can be applied as [12]:

$$A_0 * V_0 = A_1 * V_1. \quad (1)$$

Based on Eq. 1, the reduction R in csa can then be determined by the ratios of csa, as well as of process velocities, before and after the induction coil as follows [13]:

$$R = 1 - \frac{V_0}{V_1} = 1 - \frac{A_1}{A_0}. \quad (2)$$

This enables two ways of calculating R: From the measurement of diameters to determine the csa or the set process velocities, respectively. However, this is only valid for a single pass DD. For multiple passes, the overall reduction ratio R_{ov} can be determined by:

$$R_{ov} = 1 - \prod_{i=1}^{n}(1 - R_i) \text{ for n multiple passes } (n \in \mathbb{N}). \quad (3)$$

Using Eq. 3 on Eq. 2, the achieved reduction ratio R_a from the csa determination and the set reduction ratio R_s taken from the velocity ratio are calculated for a single pass i and for an overall reduction ratio for multiple passes as follows:

$$R_a = 1 - \frac{A_i}{A_{i-1}} \text{ for a single pass i,} \quad (4)$$

$$R_{a,ov} = 1 - \prod_{i=1}^{n}\frac{A_i}{A_{i-1}} = 1 - \frac{A_n}{A_0} \text{ for n multiple passes } (n \in \mathbb{N}) \text{ and} \quad (5)$$

$$R_s = 1 - \frac{V_{0,i}}{V_i} \text{ (with } V_{0,i} \text{ being the respective feeding velocity for } V_i) \text{ for a single pass i and} \quad (6)$$

$$R_{s,ov} = 1 - \prod_{i=1}^{n}\frac{V_{0,i}}{V_i} \text{ for n multiple passes } (n \in \mathbb{N}). \quad (7)$$

If the feeding velocity V_0 remains the same over all n passes, Eq. 7 can be simplified to:

$$R_{th,ov} = 1 - \frac{{V_0}^n}{\prod_{i=1}^{n} V_i}. \quad (8)$$

Materials and Experiments

As feedstock material, a wire of Mg alloy AZ31 with a thickness of 1 mm is used for all experiments. A cast ingot of the alloy was machined into cylindrical shape for the hot wire extrusion process. A direct extrusion process was applied with a billet and container temperature of 350 °C and a ram velocity of 0.2 mm/s to receive wires, using a die with 4 nozzles positioned equidistant from the center. Details on the setup can be obtained from earlier work in Nienaber et al. [14].

The flexible experimental setup for dieless wire drawing has been described in detail in an earlier work in Braatz et al. [15] and is extended by an automatic force value export and a demountable die holder for the cold drawing at room temperature experiments of the presented study. This enables multiple process setups including DD and CCD.

For the experiments, a high frequency induction generator with a maximum power capacity of 10 kW and a frequency of 1383 kHz is used, generating temperatures in the range from 200 to 400 °C by variating the input power of the induction heating coil from 1.1 to 1.6 kW. For measuring the process temperature, a radiation based thermal imaging (IF) camera is used with an accuracy of ± 10 °C. A single torque sensor on the drawing side servo motor measures the acting torques in Nm during the process, which are then converted into process forces in N and exported for every second of process time. For calculating the achieved reduction ratio R_a of the wire in Eq. 4 and 5, a minimum of five measuring points for the ingoing diameter d_0 before the coil and for the outgoing diameter d_1 several measuring points (every 5 to 10 cm) after the coil are taken. During the experiments for the DD process, the feeding velocity V_0 is fixed to 10 mm/s and the drawing velocity V_1 is set to 11.25 or 12.5 mm/s to achieve reductions in csa of 10 % or 20 %, respectively. For the CCD process, the drawing velocity is set to 10 mm/s and a die is chosen from the die set that is closest to the targeted reduction ratio R. In the setup the wires are preloaded at 15 ± 2 N, the duration of every experiment equals a 5 m sample size and each set of process parameters is applied three times.

The mechanical properties are investigated by carrying out tensile tests at ambient air temperature using an universal testing machine Zwick05 with a maximum load of 5 kN. At a constant initial strain rate of 10^{-3} s^{-1}, stress-strain diagrams and the related stress and strain properties are obtained. Standard metallographic procedures with picric acid etching are used for measuring the grain size with an Olympus light microscope and a Keyence laser scanning microscope is used for surface analysis.

Results and Discussion

Process stability. The process stability of the DD process itself is addressed by continuous analysis of the process parameters and along the length of the wire, for each experiment.

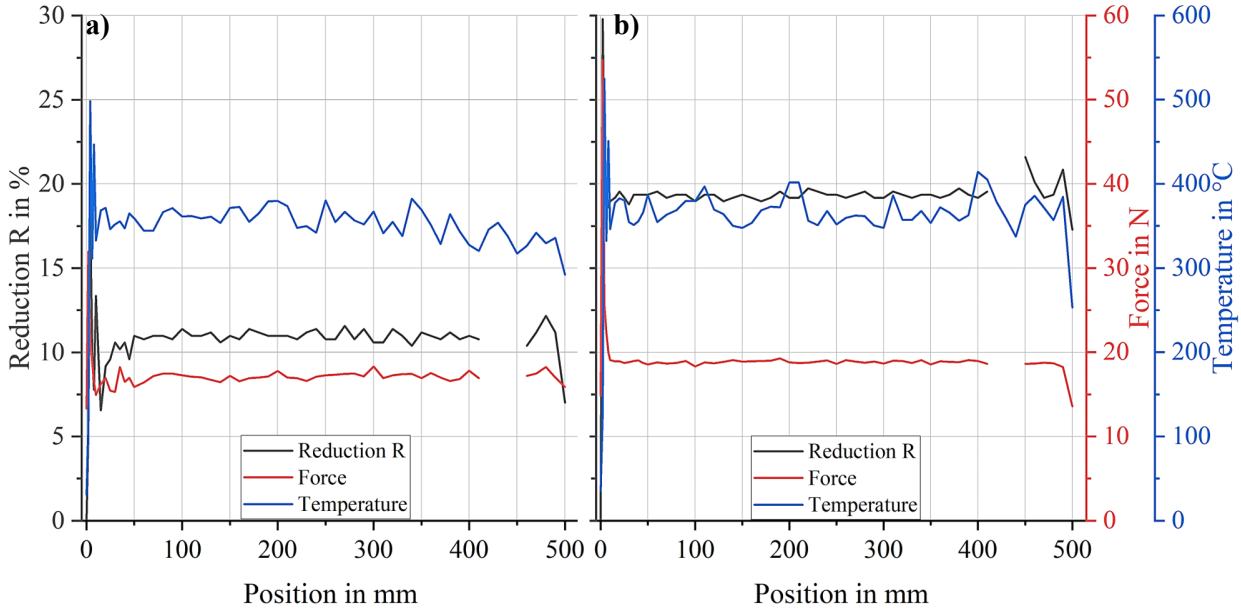

Figure 2. Process forces, temperatures and reduction ratio for single passes a) R = 10 % and b) R = 20 % at 1.5 kW.

Fig. 2 shows the variation in process forces, process temperature and the reduction ratio over the length of the wire for two representative DD processes with 10 % and 20 % reduction ratio. The gaps in the force and reduction ratio curves are due to calibration paint reference points for the emissivity calibration of the IF camera. For all DD experiments, it is observed that a steady state occurs after approx. 17 sec. For all single pass experiments with a csa reduction of 10 %, a maximum standard derivation of ± 0.014 mm in diameter and ± 3.1 N in force is measured. For all experiments with 20 % csa reduction, a maximum standard derivation of ± 0.003 mm in diameter and ± 4.5 N is obtained. The results have to be compared to a variation in diameter of ± 0.002 mm of the extruded wire, which is used as feedstock material, and a variation in process forces for CCD experiments of ± 2.35 N. Thus, the variation in diameter after a DD process is only slightly increased. This indicates an overall stable process during the steady state with even higher homogeneity regarding diameters for experiments with 20 % reduction ratio.

Process reproducibility. Secondly, the reproducibility of the DD process is investigated in comparison to the CCD process. Each experiment with fixed parameters is repeated three times to receive mean values and standard derivations of the process parameters for each parameter setting.

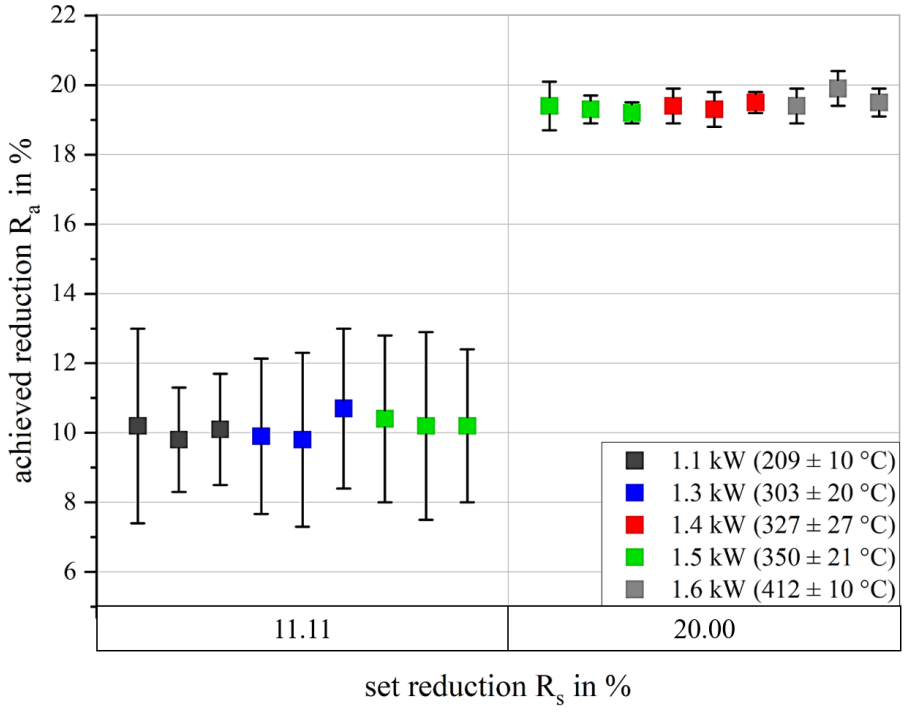

Figure 3. Achieved reduction over set reduction for all DD single pass experiments.

In Fig. 3, for each single pass DD experiment, the achieved reduction ratio R_a, calculated from Eq. 4, are compared with the set reduction ratio R_s, calculated according to Eq. 6. Focusing on each parameter set, similar results are obtained with respect to the achieved reduction ratio and variation in diameter. Temperature variations of up to 220 °C for the same reduction ratio do not appear to affect a change in the reduction ratio or the magnitude of the deviation. Taken all experiments at R_s = 11.11 %, the mean achieved reduction is 10.14 ± 2.3 %. Moreover, for all experiments at R_s = 20 %, the mean achieved reduction is 19.43 ± 0.45 %. Comparing experiments of the same parameter sets, the DD process shows the same mean values of reduction ratio, as well as force and temperature values with similar standard derivations. This indicates similar results for DD process experiments with the same process parameter settings and therefore a good reproducibility.

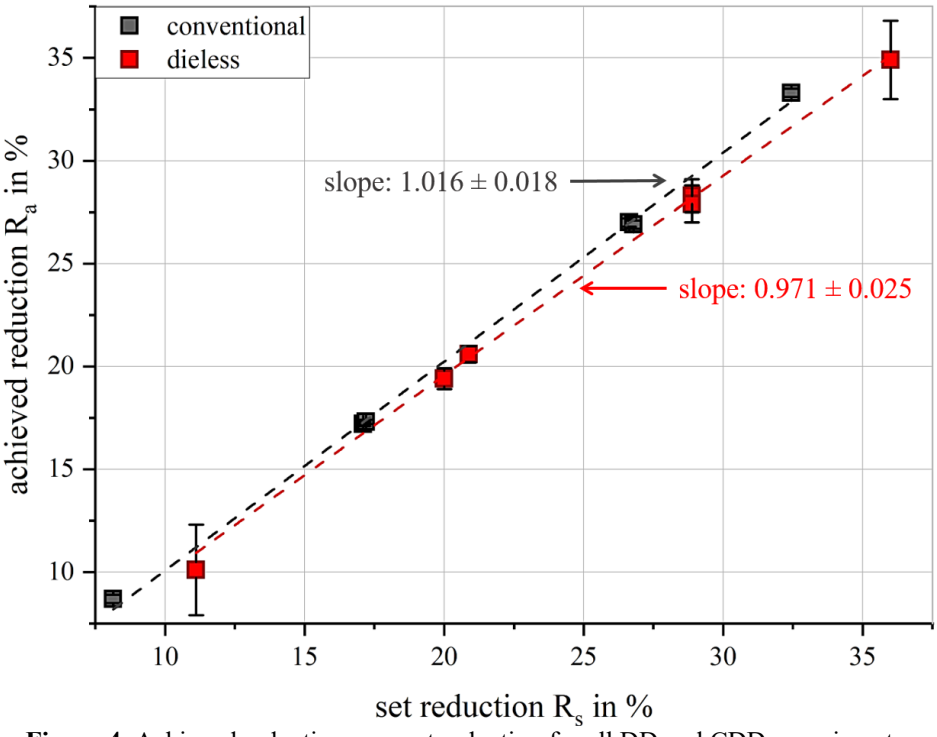

Figure 4. Achieved reduction over set reduction for all DD and CDD experiments.

Fig. 4 compares the overall achieved and set reduction ratios for each parameter setting for all DD and all CCD experiments. For the CCD experiments a standard derivation of maximum ± 0.002 mm in diameter is revealed for all reduction ratios, whereas the DD experiments have the highest magnitude in standard derivation in diameter (± 0.017, respective ± 0.030 mm) for set reductions of 11.11% and 36 % and the lowest magnitude (± 0.007, respective ± 0.016 mm) for 20 % and 20.98 %. Linear regression of all data for the DD and the CCD experiments results in a slope of approx. 1 for the CCD experiments as expected. For the DD experiments, the values of R_a are slightly lower than the values of R_s and the regression curve follows a line with a slope of 0.971 and is therefore also close to 1 with only a slightly higher derivation then the one for CCD. This indicates that the reduction in csa for the DD process can be accurately adjusted through process parameter variation.

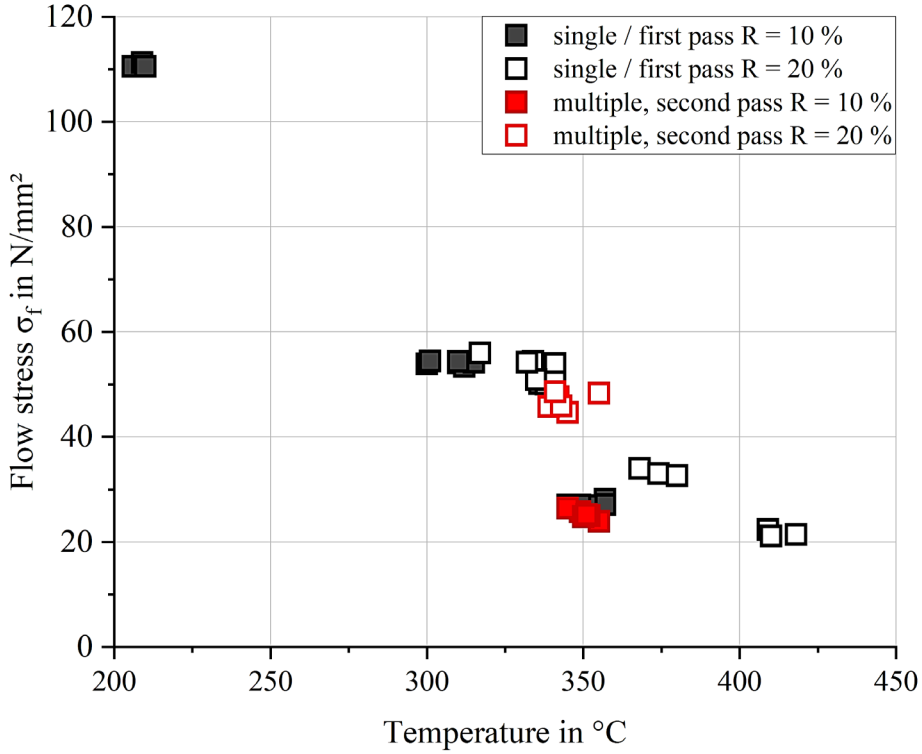

Figure 5. Flow stress over process temperature for all DD experiments.

For calculating the flow stress, the average process force F and the determined final csa A_1 are used. Fig. 5 shows the flow stress σ_f over the process temperature for all single and multiple (double) passes DD experiments for different reduction ratios. In general, a tendency of lower process flow stresses for higher temperatures can be observed. Higher reductions also lead to an expected increase of the process forces or the flow stresses, respectively, which is consistent for the higher temperature range applied in this study. It is interesting to note that the flow stresses for a single drawn wire and the flow stresses for a pre-drawn wire (shown in red) do not differ much from each other for similar reductions and temperatures. This suggests that the property profile of the wires is not significantly affected after the first drawing pass of the DD process.

Mechanical properties. The mechanical properties of the drawn wires are studied by comparing their stress-strain diagrams and their related mechanical properties.

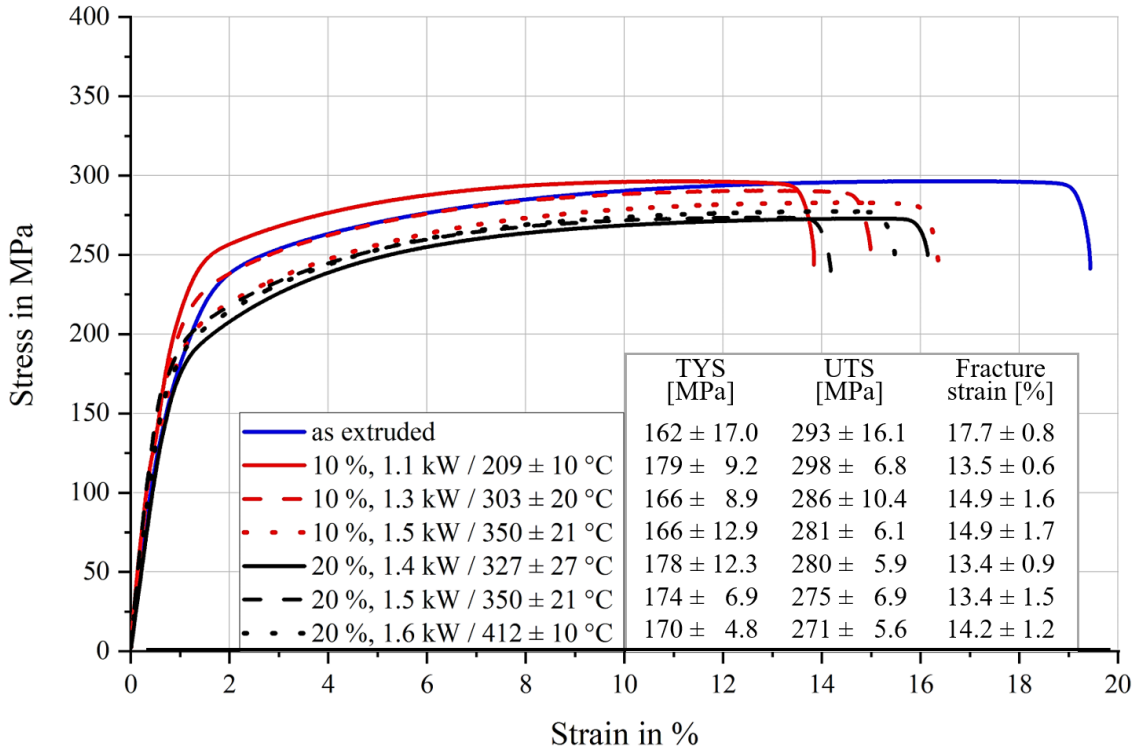

Figure 6. Stress-strain curves for starting material and DD single pass experiments.

In Fig. 6, the tensile test results for the starting material and the single pass DD experiments are plotted. For each parameter set (each carried out three times), at least three tensile tests were carried out and the mean tensile yield strength (TYS), ultimate tensile strength (UTS) and fracture strains are determined. One representative stress-strain-curve for each parameter set is shown. The average values and standard deviations for TYS, UTS and fracture strain for one parameter set show little variation within the relatively high standard deviations achieved. The fracture strains appear only slightly reduced compared to the original extruded wire before drawing. The impression of decreasing TYS and UTS with increasing input power fits to the concurrent increase of the processing temperature, but is not clear due to the high standard deviations. Still, even with a temperature variation of up to 220 °C for one reduction ratio, it is remarkable that there is no distinct impact on the resulting mechanical property profile, which remains rather stable during the drawing passes.

Table 1. Tensile test results of DD and CCD experiments.

Process	*Reduction*	*TYS in MPa*	*UTS in MPa*	*Fracture strain in %*
as extruded	-	162 ± 17.00	293 ± 16.10	17.70 ± 0.8
DD single pass	10 %	167 ± 10.36	288 ± 7.77	14.43 ± 1.3
DD single pass	20 %	174 ± 8.01	275 ± 6.16	13.67 ± 1.2
DD multiple pass	10 % + 10 %	172 ± 4.94	277 ± 6.64	14.10 ± 0.9
DD multiple pass	10 % + 20 %	191 ± 7.01	286 ± 9.47	11.10 ± 1.2
DD multiple pass	20 % + 10 %	166 ± 5.11	265 ± 7.76	13.20 ± 1.0
DD multiple pass	20 % + 20 %	191 ± 3.77	276 ± 7.76	9.50 ± 1.0
CCD single pass	10 %	224 ± 17.20	326 ± 6.69	5.30 ± 1.1
CCD single pass	20 %	222 ± 4.12	361 ± 6.57	5.30 ± 1.2
CCD multiple pass	10 % + 10 %	214 ± 11.70	346 ± 5.26	5.10 ± 0.7
CCD multiple pass	10 % + 20 %	229 ± 14.80	375 ± 6.14	3.80 ± 0.4
CCD multiple pass	20 % + 10 %	230 ± 14.90	382 ± 5.12	4.20 ± 0.4
CCD multiple pass	20 % + 20 %	243 ± 18.80	285 ± 8.71	3.90 ± 0.3

Tab. 1 lists the results of the mechanical values for all DD and CCD experiments, where the DD single pass experiments at different temperatures for reduction ratios of 10 % and 20 % are summarized.

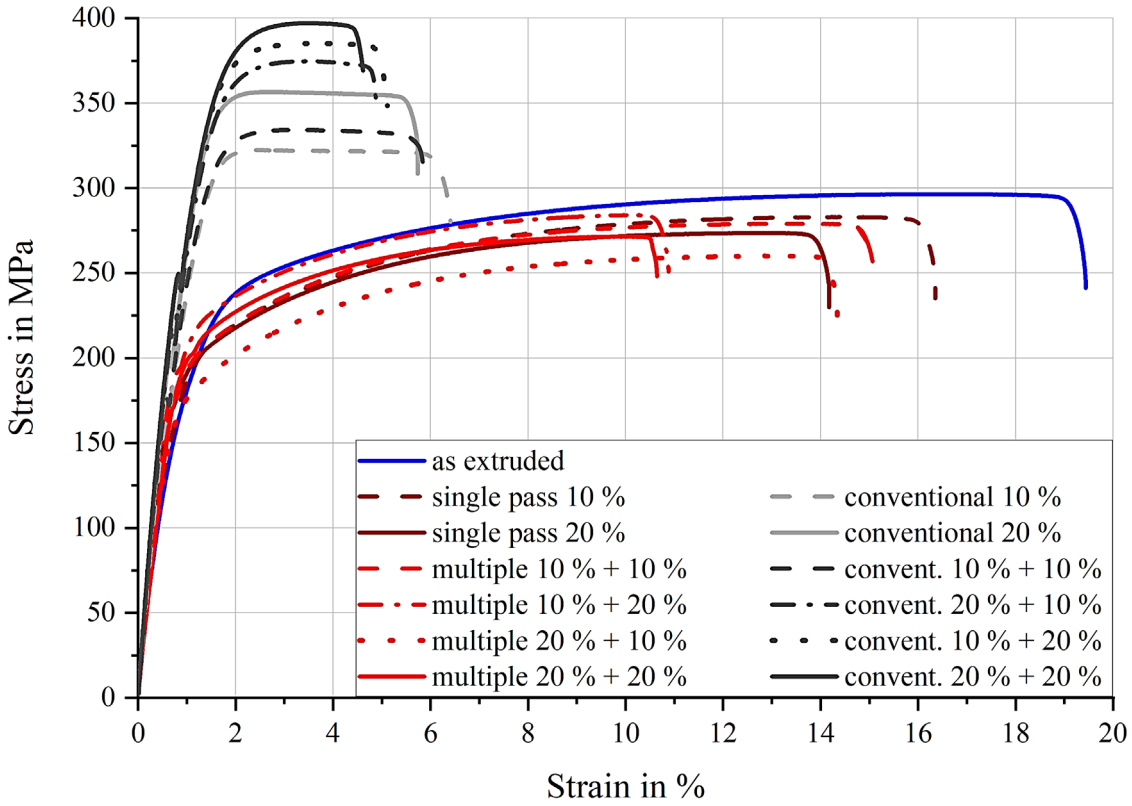

Figure 7. Stress-strain curves for starting material and all DD and CCD experiments.

For Fig. 7, representative stress-strain-curves for every parameter set for DD and CCD experiments are plotted. In the comparison of the DD and the CCD experiments in general, it stands out, that the DD experiments have slightly increasing TYS, mostly unaffected UTS and slightly decreasing fracture strain with increasing reduction ratio compared to the starting material, while the CCD results have significantly higher TYS and UTS and substantially lower fracture strain. These changes in TYS, UTS and fracture strain are well related to the work hardening of the material during the drawing passes of the CCD process. Focusing on the CCD experiments, the fracture strain is decreasing slightly and the TYS is increasing slightly over all reduction ratios, but the UTS increases significantly. Generally, the higher the reduction ratio, the higher the UTS. However, achieving the same overall reduction by adding a second pass, e.g. reaching 20 % by applying two passes of 10 %

+ 10 %, results in lower UTS. This shows that the higher the reduction in csa in a single pass, the more pronounced the work-hardening effects in the AZ31 wires, and that with multiple passes the overall reduction is still decisive. However, UTS for 10 % + 10 % remains visibly below a single pass of 20%. For 10 % + 20 % and 20 % + 10 %, the former, with a higher R value in the second pass, is more ductile than the latter.

It is interesting to note that although the elongation at fracture remains far below the values of the starting material, the various drawing steps do not significantly change it. The results also show that only one single pass with a reduction ratio of 10 % significantly changes the mechanical properties of the wire compared to the starting material. Focusing on the DD experiments, the TYS shows no significant changes, while the UTS changes slightly and the fracture strain varies with different reductions in csa. The UTS changes by a magnitude of 20 MPa and the fracture strain varies from 9.5 % (R = 20 % + 20%) to 14.9 % (R = 10 %). Generally, the lower the overall reduction, the less the difference in fracture strain compared to the 17 % of the extruded AZ31. Contrary to the CCD results, the DD curves show no significant changes for achieving 20 % reduction in a single pass or with multiple passes, whereas the order of reduction for R_s = 28.9% (10 % + 20 % or 20 % + 10 %) seems to play a role. This demonstrates that the DD process maintains the property profile of the extruded wire to a large scale while reducing its diameter.

Wire characterization. Surface and microstructure analysis of the wires are shown by means of metallographic analysis for measuring the surface roughness and the grain size.

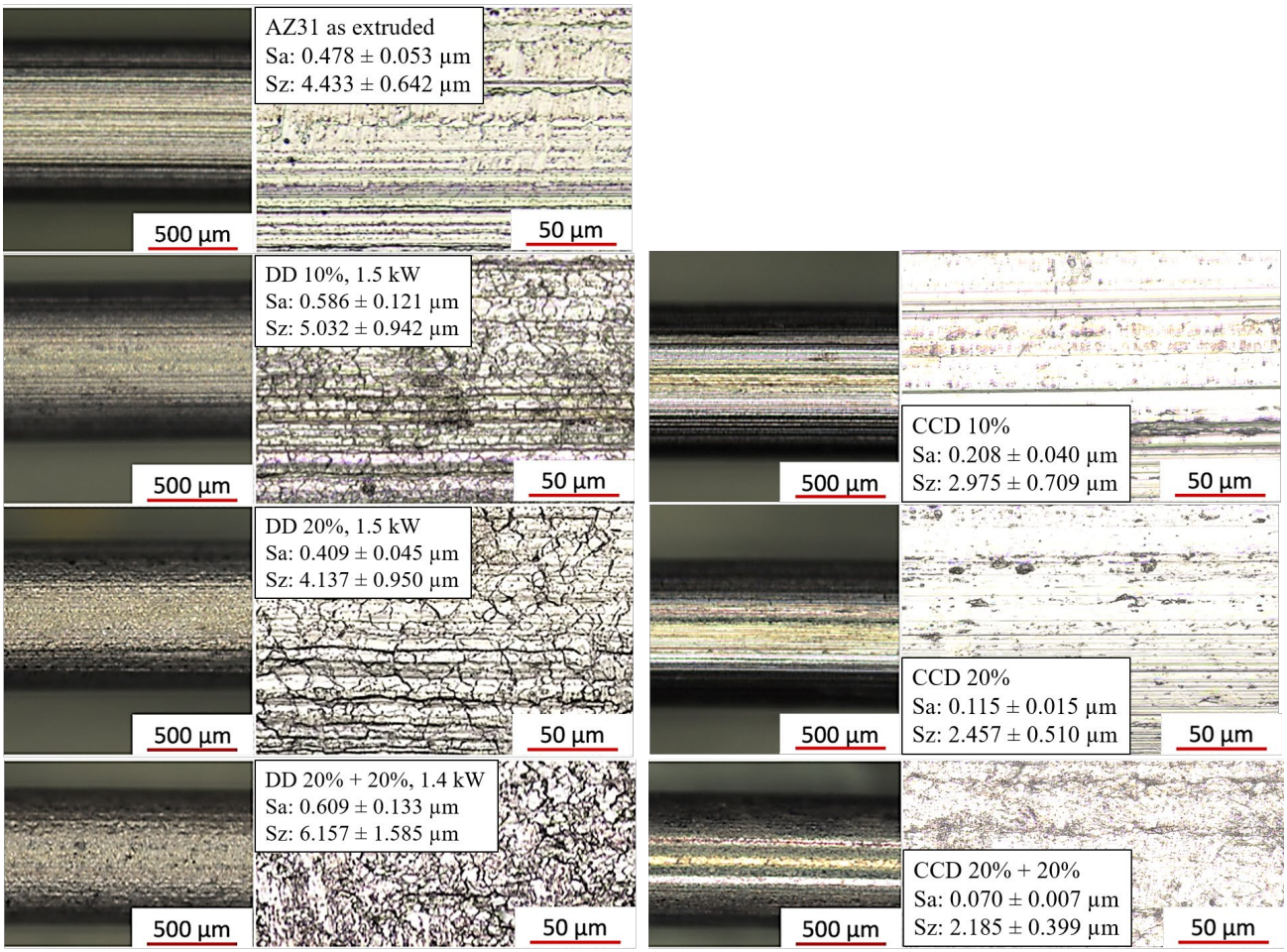

Figure 8. Laser scanning microscope analysis of starting material and selected DD and CCD experiments.

Fig. 8 displays the optical analysis with surface roughness measurements of Sa (mean arithmetic) and Sz (maximum magnitude) for the extruded and the drawn wires for single pass 10 % and 20 % and multiple pass 20 % + 20 % reduction ratio. After the DD process, the surfaces of the drawn wires are slightly rougher then the starting material, whereas the CCD wires have a significant smoother

surface than the DD wires and the extruded wire, demonstrating the positive influence of a form giving tool (die).

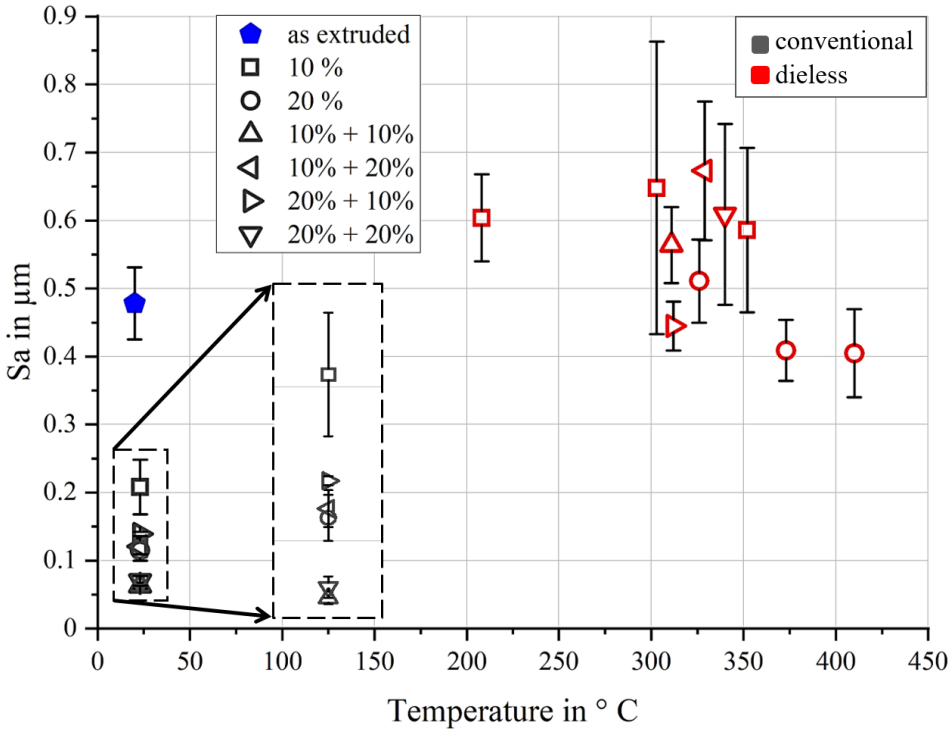

Figure 9. Arithmetic surface roughness over process temperature for all DD and CCD experiments.

Fig. 9 shows the arithmetic surface roughness Sa over the process temperature for the extruded, the CCD, and DD drawn wires. Following the findings from Fig. 8, the CCD process generally improves the surface roughness significantly while the DD process influences the surface roughness of the wires only slightly. Differences in Sa values and its deviations for different reductions in csa for the CCD may be explained by manufacturing inaccuracies of the die. For the DD wires, a tendency of slightly less rougher surfaces for higher temperatures can be observed. Higher reduction ratios seem to have an influence on the surface roughness in general and the order of reduction (e.g. 10 % + 20 % or 20 % + 10 %) seems to play a role in this context, too. This confirms that the die provides a significant surface improvement, but also indicates that the DD process does not significantly degrade the surface quality of the starting material.

As seen in Tab. 2 and Fig 10, the metallographic results show a typical AZ31 microstructure [14], which is completely recrystallized and homogeneous, for the extruded material. The drawing experiments reveal also recrystallized microstructures, which are clearly developed if the reduction R is low at 10 % and the temperature is higher than 300 °C. If the reduction R is higher at 20 %, developing grain structures with serrated boundaries can be revealed at the same temperature, too. This applies also for the double pass experiments. A temperature range of 325 to 350 °C reveals rather homogeneous microstructures with average grain size of 7 to 8 µm. Higher temperature, e.g. in Fig. 10 m), shows increasing grain size, here up to 12 µm. Multiple pass DD experiments seem to very slightly increase the average grain size to 7 to 9 µm. Grain size analysis for CCD drawn wires reveal a deformed version of the initial microstructure of the extruded wires, where the etching impact increases on other obstacles than the grain boundaries due to the work hardened condition of the wires. The average grain size appears unchanged as expected in Fig. 10 b) and 10 c). Higher CCD reductions of the csa are strongly deformed and do not offer the possibility of grain size quantification (Fig. 10 d) - g)).

Table 2. Variation of grain size for specimens of DD and CCD process.

№	*Process*	*Reduction ratio R in %*	*Temperature in °C*	*Grain size in µm*
a)	as extruded	-	-	6 ± 1
b)	CCD single pass	10	20	6 ± 1
c)	CCD single pass	20	20	(6 ± 1)
d)	CCD multiple pass	10 + 10	20	-
e)	CCD multiple pass	10 + 20	20	-
f)	CCD multiple pass	20 + 10	20	-
g)	CCD multiple pass	20 + 20	20	-
h)	DD single pass	10	209 ± 10	6 ± 1
i)	DD single pass	10	303 ± 20	5 ± 1
j)	DD single pass	10	350 ± 21	7 ± 1
k)	DD single pass	20	327 ± 27	7 ± 1
l)	DD single pass	20	350 ± 21	8 ± 1
m)	DD single pass	20	412 ± 10	12 ± 1
n)	DD multiple pass	10 + 10	303 ± 20	9 ± 1
o)	DD multiple pass	10 + 20	303 ± 20 & 327 ± 27	7 ± 1
p)	DD multiple pass	20 + 10	327 ± 27 & 303 ± 20	9 ± 1
q)	DD multiple pass	20 + 20	327 ± 27	7 ± 1

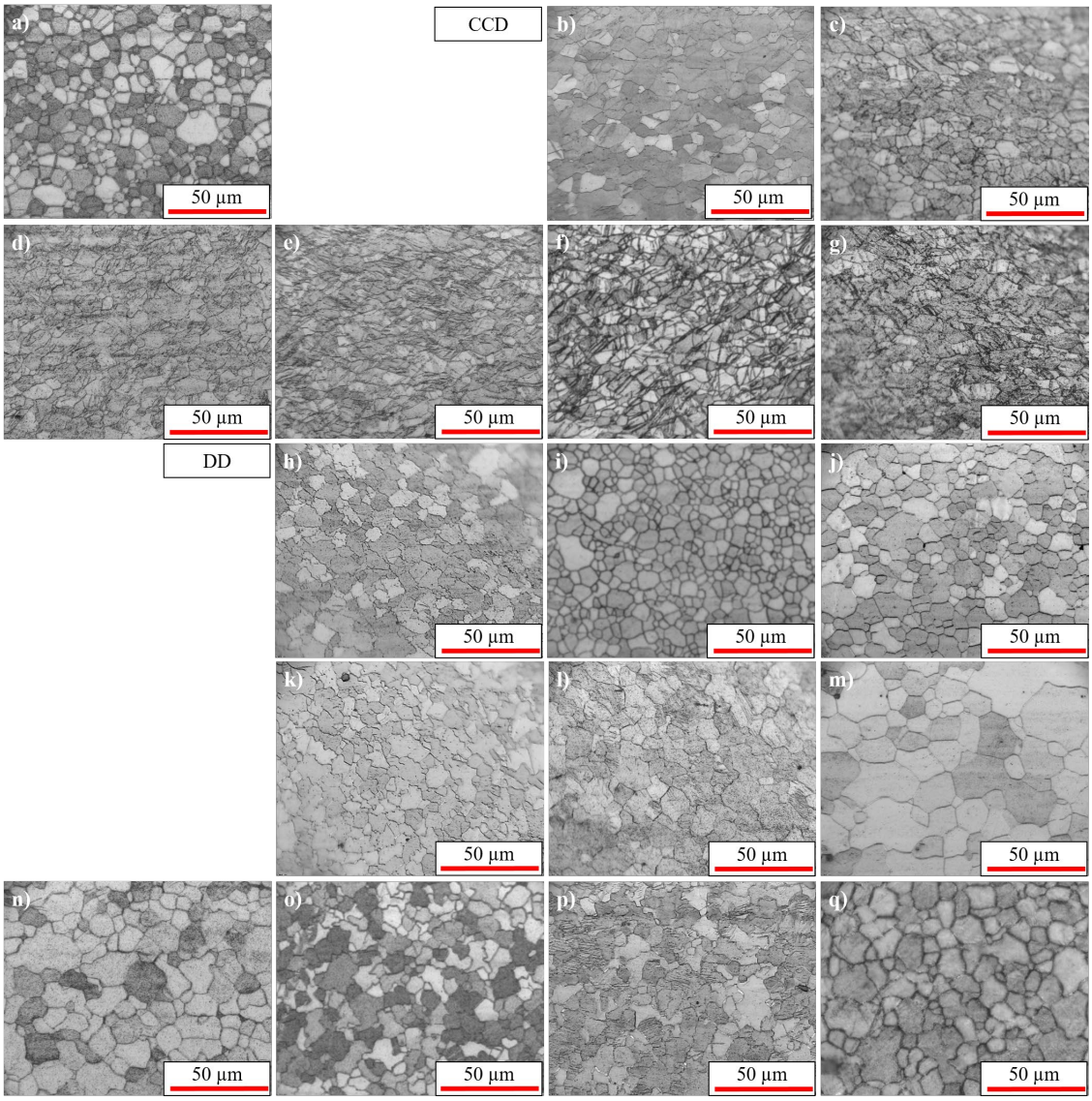

Figure 10. Micrographs from longitudinal sections for AZ31 wires for Table 2.

Conclusion

In this study, the process stability and reproducibility of the DD process for AZ31 magnesium wires was investigated. The following results were obtained:

1. The DD process indicates an overall stable process after reaching the steady state.
2. Close results in terms of accuracy for DD process experiments with the same process parameter settings re obtained after being carried out multiple times indicating a good reproducibility.
3. An overall reduction in csa for the DD process, single and multiple pass, can be accurately adjusted through process parameters.
4. The DD process shows no distinct impact on the resulting mechanical property profile of the AZ31 wires, even for temperature variations of up to 220 °C.
5. The die in a CCD process provides a significant surface improvement, while the DD process seems to not significantly affect the surface quality of the starting material.
6. Overall, the DD process maintains the property profile of the starting material to a large extend.

Acknowledgments

The authors would like to thank Mrs. Maria Nienaber for her help with the extrusion of the wires and Mr. Chee Hans Ho for his help with carrying out wire drawing experiments and surface measurements. Furthermore, the authors would like to thank Mr. Axel Dieckmann for his valuable comments and his prior work with the design of the experimental setup.

References

[1] V. Weis, R.A. Kot, Dieless Wire Drawing with Transformation Plasticity, Wire Journal (9), (1969) 182–189.

[2] H. Sekiguchi, K. Kobatake, K. Osakada, A Fundamental Study on Dieless Drawing. In: S.A. Tobias, F. Koenigsberger (Eds.) Proceedings of the Fifteenth International Machine Tool Design and Research Conference. Palgrave, London, 1975, pp. 539–544. https://doi.org/10.1007/978-1-349-01986-1_63.

[3] R. Fortunier, H. Sassoulas, F. Montheillet, A thermo-mechanical analysis of stability in dieless wire drawing, International journal of mechanical sciences (39, 5), (1997) 615-627. https://doi.org/10.1016/S0020-7403(96)00060-4.

[4] P. Tiernan, M.T. Hillery, Dieless wire drawing - an experimental and numerical analysis, Journal of Materials Processing Technology (155), (2004) 1178-1183. https://doi.org/10.1016/j.jmatprotec.2004.04.175.

[5] M.D. Naughton, P. Tiernan, Requirements of a dieless wire drawing system, Journal of materials processing technology (191.1-3), (2007) 310-313. https://doi.org/10.1016/j.jmatprotec.2007.03.054.

[6] T. Furushima, K. Manabe, Experimental and numerical study on deformation behavior in dieless drawing process of superplastic microtubes, Journal of Materials Processing Technology (191.1-3), (2007) 59-63. https://doi.org/10.1016/j.jmatprotec.2007.03.084.

[7] T. Furushima, S. Hirose, K. Manabe, Effective temperature distribution and drawing speed control for stable dieless drawing process of metal tubes, Journal of Solid Mechanics and Materials Engineering (3.2), (2009) 236-246. https://doi.org/10.1299/jmmp.3.236.

[8] A. Milenin, et al., Computer aided design of the laser dieless drawing process of tubes from magnesium alloy with take into account ductility of the material, Procedia Manufacturing (15), (2018) 302-310. https://doi.org/10.1016/j.promfg.2018.07.223.

[9] A. Milenin, et al., Improving the workability of materials during the dieless drawing processes by multi-pass incremental deformation, Archives of Civil and Mechanical Engineering (20.3), (2020) 1-14. https://doi.org/10.1007/s43452-020-00092-4.

[10] J.-M. Seitz, E. Wulf, P. Freytag, D. Bormann, F.-W. Bach, The Manufacture of Resorbable Suture Material from Magnesium. In Adv. Eng. Mater. 12 (11), (2010) 1099–1105. https://doi.org/10.1002/adem.201000191.

[11] V.S. Hristov, K. Yoshida, Benefits of Using Diamond Dies for Cold Alternate Drawing of Magnesium Alloy, Key Engineering Materials (716), (2016) 13-21. https://doi.org/10.4028/www.scientific.net/kem.716.13.

[12] J. Dietrich, J., Praxis der Umformtechnik: Umform- und Zerteilverfahren, Werkzeuge, Maschinen, Springer-Verlag, 2017, pp 113-114.

[13] P. Tiernan, M. T. Hillery, An analysis of wire manufacture using the dieless drawing method, Journal of Manufacturing Processes 10 (1), (2008) 12–20. https://doi.org/10.1016/j.manpro. 2008.05.001.

[14] M. Nienaber, S. Yi, K.U. Kainer, D. Letzig, J. Bohlen, On the Direct Extrusion of Magnesium Wires from Mg-Al-Zn Series Alloys, Metals 10 (9), (2020) 1208. https://doi.org/10.3390/met10091208.

[15] M. Braatz, A. Dieckmann, J. Bohlen, N. Ben Khalifa, Experimental Setup of Dieless Drawing Process for Magnesium Wire. In: Behrens BA., et al. (Eds.) Production at the Leading Edge of Technology. WGP 2021. Lecture Notes in Production Engineering. Springer, Cham, 2021, pp. 38-46. https://doi.org/10.1007/978-3-030-78424-9_5.